American Mineralogist, Volume 83, pages 1220–1230, 1998

Molecular dynamics simulations of molten $CaAl_2Si_2O_8$: Dependence of structure and properties on pressure

DEAN NEVINS[1,*] AND FRANK J. SPERA[1,2]

[1]Department of Geological Sciences, University of California, Santa Barbara, California 93106, U.S.A.
[2]Institute for Crustal Studies, University of California, Santa Barbara, California 93106, U.S.A.

ABSTRACT

Molecular dynamics (MD) simulations were carried out on molten $CaAl_2Si_2O_8$ at nine pressures from 0.2 to 76 GPa at 4000 K, well above the computed glass transition temperature. A simple effective pair-potential with both Coulombic interaction and Born-Mayer-Huggins short-range repulsion was used. Simulations of duration 30 ps long were performed in the microcanonical ensemble (NEV) utilizing 1300 particles (O+Ca+Si+Al). As pressure increases, profound changes occur in the relative abundance of $^{[4]}$T, $^{[5]}$T, $^{[6]}$T, $^{[7]}$T, and $^{[8]}$T (T = Si,Al) as well as in the coordination of Ca by O. At low pressure, most T are in fourfold coordination with oxygen, oxygen is twofold coordinated to T, and Ca has six to seven nearest O atom neighbors. At 5 GPa, where $^{[5]}$T maximizes, more than half of the T atoms are pentahedrally coordinated ($^{[5]}$T) in distorted trigonal bipyramids. Both $^{[4]}$T (25%) and $^{[6]}$T (18%) are present at 5 GPa and change rapidly as pressure increases ($^{[4]}$T decreases and $^{[6]}$T increases). At 5 GPa, the average coordination number (CN) of oxygen about Ca is 8. At 20 GPa, $^{[6]}$T constitutes more than 50% of the TO_n subunit population and the CN of oxygen around Ca is 10. At medium range (3 to 10 Å), the most significant change in melt structure as pressure increases is replacement of corner-sharing ring-former TO_n polyhedra with edge-sharing polyhedra pairs such as TO_5-TO_6 and TO_6-TO_6. The destruction of the ring structure correlates with the maximization of Ar solubility as pressure increases. Ring structure collapse is geometrically captured by variation in the distribution of T-O-T angles with increasing pressure. The low-pressure maximum at 140° with large variance agrees with X-ray data and follows from the distribution of *N*-member rings with *N* ranging from 4 to 8 (or larger). At higher pressure, the T-O-T distribution narrows and shifts toward smaller angles around 105° consistent with the dominating presence of edge sharing between TO_6-TO_6 and TO_5-TO_6 pairs. Tracer diffusivities for O, Ca, Al, and Si increase at low pressure as pressure increases. The diffusivity of oxygen correlates with ring collapse and attains a maximum at 5 GPa ($D_{ox} = 6.6 \times 10^{-9}$ m^2/s); the ratio of diffusivities for Ca, Al, and Si relative to oxygen are 0.67, 0.62, and 0.51, respectively. These data suggest that pentahedrally coordinated T acts as an ''activated complex'' for oxygen diffusion. Below 5 GPa, activation volumes (V^*) for all species are large in absolute value and lie in the range -25 to -35 cm^3/mol; these are similar in absolute value to the partial molar volume of Ar in molten $CaAl_2Si_2O_8$ of 22 cm^3/mol. The large absolute values for V_a at low pressure correlate with the contribution to the isothermal compressibility made by configurational effects inferred from Brillouin scattering experiments. At higher pressure, the anomalous diffusion disappears. V_a decreases for all species in absolute value and changes sign; at 20 GPa, V_a is about $+3$ cm^3/mol, much smaller than the partial molar volume of Ar in molten anorthite.

INTRODUCTION

The properties of molten silicates at high pressure and temperature are relevant to several important Earth science problems, including the dynamics of the deep mantle, the fate of subducted oceanic crust, and the evolution of the Hadean magma ocean on the early Earth. Because melt properties are largely governed by the topological characteristics of atomic packing, the structural response of a silicate liquid to high temperature and pressure is of interest. The typical arrangement of four O atoms around each T atom ($^{[4]}$T), where T is either silicon or aluminum, and the coordination of two T around each O atom ($^{[2]}$O) in both crystalline and molten silicates gives way to more highly coordinated units as pressure increases (e.g., see Stebbins and Mcmillan 1989 and Wolf and McMillan 1995 for an excellent review). However, significant ques-

* E-mail: d.nevins@ieee.org

0003–004X/98/1112–1220$05.00

tions remain concerning the role of fivefold- and higher-coordinated T and the related bonding environment of oxygen on liquid transport, spectroscopic, and thermodynamic properties. Similarly, the detailed effects of pressure on short and intermediate range order in molten silicates has not been extensively investigated, although it is clear that marked changes do occur (e.g., see Rustad et al. 1991 for effects in silica).

We have performed molecular dynamics (MD) simulations of molten $CaAl_2Si_2O_8$ at 4000 K and pressures ranging from 0.2 to 76 GPa to study changes in short and medium range order and to correlate structural changes with the pressure dependence of tracer diffusivity (O, Ca, Al, and Si) and other material properties including the solubility of Ar. The potential used to characterize bonding in the MD simulations is a simple, pair-wise additive Born-Mayer-Huggins potential that features Coloumbic interaction and short-ranged repulsion. We recognize the inherent limitations implied by such a simple potential in explaining the structure and properties of molten and glassy silicates. Three-body forces, directional bonding, polarizability, and other effects are arguably important. Yet, work over the past two decades (e.g., see Woodcock et al. 1976; Matsui and Kawamura 1984; Rustad et al. 1990; Kubicki and Lasaga 1993; Poole et al. 1995; Stein and Spera 1995, 1996; Bryce et al. 1997) supports the notion that MD simulations play a useful role in providing insight regarding mechanisms and posing structural and dynamic questions amenable to experimental exploration and even making semi-quantitative predictions regarding large-scale Earth processes. The simple effective ionic pair-potential used here has the advantage of containing few adjustable parameters and allows a simple and clear physical interpretation.

Plagioclase, or its hydrated analog, is an important component within subducted gabbroic oceanic crust and within feldspar-rich continental crust. Phase equilibria studies by Gautron et al. (1996) led to the conclusion that if plagioclase-rich compositions are transported to transition zone depths (about 25 GPa) and encounter ambient mantle temperatures, partial melting can be expected. Although it is unlikely that these melts would be erupted, such low-viscosity melts could confer crustal trace element and isotopic signatures to mantle peridotite by metasomatic reaction. An additional reason for studying molten anorthite is that many thermodynamic, X-ray, and spectroscopic data are available; predictions based on MD simulations can be compared with laboratory results.

Methods

The code used to perform the MD simulations is based on a collection of FORTRAN routines from Allen and Tildesley (1987) modified by Rustad et al. (1990, 1991) and Stein and Spera (1995, 1996). Post-processing programs to evaluate thermodynamic and transport properties were modified from Stein and Spera (1995). New codes to determine coordination statistics and extract polyhedra for visualization were developed for this investigation. Polyhedra visualization was provided by ATOMS (Dowty 1995). Simulations were run on local IBM RS/6000 workstations and the NERSC CRAY C-90 super computer located at the Lawrence Livermore National Laboratory. The number of particles used in all numerical experiments was 1300; earlier studies using the same potential have shown that smaller numbers of particles, <900, are insufficient for calculating both static and dynamic properties (Kawamura 1991; Stein and Spera 1995). Experiments were typically 30 ps in length to obtain adequate mean-square displacements and ion diffusivities. The intermolecular potential used was the simple Born-Mayer-Huggins type $U_{ij} = q_i q_j / r_{ij} + A_{ij} \exp(-B_{ij} r_{ij})$, where q_i is the ionic charge of the i^{th} ion, q_j is the ionic charge of the j^{th} ion, r_{ij} is the interatomic bond distance between ions i and j, and A_{ij} and B_{ij} are the short-range potential parameters. The potential parameters A_{ij}, B_{ij}, and q (Table 1) are identical to the parameters given by Scamehorn and Angell (1991) though expressed differently. The Coulombic interaction was computed using Ewald's method with $K = 5/L$ (the convergence parameter describing the width of the Gaussian canceling distribution surrounding each ion) where L is the length of one side of the primary MD cell. The reciprocal space portion of the sum was limited to reciprocal lattice vectors $\boldsymbol{\kappa} = 2\pi\mathbf{n}/L$ such that $|n|^2 \leq 81$. Short-range repulsive forces were cutoff at a distance of 10 Å. All simulations were performed with the constraints of constant particle number, volume and energy (NEV ensemble) for 30 ps using a 1 fs time step. Energy and momentum was conserved to better than 1 part in 10^6. Particle positions and velocities were saved every 100 fs for post-processing analysis.

Table 1. Potential parameters

Species i	Species j	A_{ij} ($\times 10^{-9}$ erg)	B_{ij} ($\times 10^{8}$ cm^{-1})
Ca	Ca	15.387	3.4483
Al	Ca	7.7528	3.4483
Al	Al	3.8831	3.4483
O	Ca	5.9082	3.4483
O	Al	3.0913	3.4483
O	O	1.7014	3.4483
Si	Al	3.7906	3.4483
Si	Ca	7.6069	3.4483
Si	O	3.1295	3.4483
Si	Si	3.6839	3.4483

Note: Computed from the parameters given in Scamehorn and Angell (1991). Formal ionic charges were used, q = +2 for Ca, +3 for Al, +4 for Si, and −2 for O.

Initial particle positions and velocities were generated randomly; this causes large repulsive forces to develop in the system. These forces were allowed to first relax before the temperature was dropped to 10 000 K, and the system was allowed to thermally equilibrate for 10 ps to attain a Maxwellian distribution of velocities and constant total energy. Excess linear momentum was then removed from the system and the thermal cycle was begun from a thermally equilibrated initial state of 10 000 K. The temperature was dropped to 4000 K in 10 ps (a rate of

6.0×10^{14} K/s) and allowed to pressure equilibrate to about 1 GPa. Vollmayr et al. (1996) showed that cooling rate has a small effect on structure and properties of silica glass utilizing a potential similar to the one used here. This effect should be less for $CaAl_2Si_2O_8$ because of its lower glass transition temperature. The MD simulations were conducted along the 4000 K isotherm, which is well above the estimated computed glass-transition temperature of 2300 K for molten $CaAl_2Si_2O_8$.

A simple calculation reveals that the structures and properties determined here apply to the relaxed state of liquid anorthite. Oxygen self-diffusivity (D) can be approximately converted to melt viscosity (η) using the Eyring relation $\eta = kT/\lambda D$ where λ corresponds to the distance of the first peak in the O-O pair correlation function and k is Boltzman's constant. The Maxwell shear relaxation time (τ) is given by $\tau = \eta/G$ where G is the modulus of rigidity, which is about 25 GPa for molten anorthite (Bansal and Doremus 1986). Computed shear relaxation times are on the order of 1 ps or less for the MD simulations, far shorter than the experiment duration of 30 ps, ensuring that all calculated structures and properties are fully relaxed.

The 1 GPa configuration formed the basis for the 1 GPa production run, and it also acted as the starting point for other experiments by suitable change in the volume of the primary MD cell. For example, to obtain the 4.8 GPa initial configuration, the pre-production configuration at 1 GPa was compressed by reducing the box size at the constant rate of 0.001 GPa/fs for 3800 fs. The resultant 4.8 GPa configuration was used as the basis for both the production run at 4.8 GPa and as the starting point for the 10.8 GPa configuration. The initial configurations for experiments at pressures of 0.2, 1.6, 25.3, 39.6, 57.9, and 75.8 GPa were generated similarly.

Results

Short-range structures

Short-range structure is determined by statistical analysis of partial pair correlation functions (the so-called radial distribution function, RDF) between two species according to:

$$g(r) = \frac{V}{N^2}\left\langle \sum_{i=1}^{N} \sum_{j=1, j\neq i}^{N} \delta(r - r_{ij}) \right\rangle \quad (1)$$

This expression finds the normalized distribution of one species around another throughout the primary MD box and its periodic extensions within a specified cut-off distance. V is the volume of the MD cell and N the number of particles. The brackets denote ensemble averaging. By numerical integration of the RDF, one may determine coordination numbers for any atom of interest. An O atom is considered coordinated to Si provided it lies within the distance of the first minimum of the RDF for O about Si. Likewise, O is considered coordinated to Ca provided it lies within the distance of the first minimum of the RDF for O about Ca. Due to compression, the first minimum of the RDFs shifts as pressure increases; this has been incorporated into the pair correlation analysis to avoid spurious ''over-coordination.''

Structure is quantified through the linkages of the atoms. Short-range order of T cations about oxygen is labeled such that $^{[1]}$O refers to nonbridging oxygen (NBO), $^{[2]}$O is the common twofold-coordinated oxygen environment ubiquitous in low-pressure network crystalline and molten silicates, and $^{[3]}$O is oxygen with three nearest T neighbors as, for example, in the crystalline phase stishovite. Intermediate range order, at 4 to 8 Å, is defined by how the short-range units such as TO_4, TO_5, TO_6, etc. are linked. In general, $^{[4]}$T is an excellent ring-former; $^{[5]}$T plays an amphoteric role in that it can link to a $^{[4]}$T or another $^{[5]}$T to form rings or it can edge share with $^{[6]}$T and not participate in ring formation. TO_6 octahedra have a propensity to edge share and not take part in ring formation (see below).

The number fraction of various T species as a function of pressure at 4000 K are depicted in Figure 1a. Because there is relatively little fractionation of Al and Si in TO_n polyhedra, Si and Al are grouped together and referred to as T. The slight partitioning of Al is discussed under ''diffusion'' below. At low pressure (0.2 GPa), melt is dominated by $^{[4]}$T consistent with previous X-ray and spectroscopic studies (e.g., Taylor and Brown 1979; McMillan and Wolf 1995 and references therein). As pressure increases to 5 GPa, there is a rapid decrease in $^{[4]}$T and concomitant increase in both $^{[5]}$T and $^{[6]}$T. At 1 GPa Scamehorn and Angell (1991) similarly calculated an average coordination of 4.2. Pentahedral T attains a maximum at 5 GPa where it equals 55% of the species present compared to 22% for both $^{[4]}$T and $^{[6]}$T. The compression ratio, defined as V_0/V where V is the molar volume of the liquid and V_0 is the molar volume at 0.2 GPa, is 1.2 at 5 GPa. That is, the molar volume of $CaAl_2Si_2O_8$ melt at the pressure of the maximum abundance of TO_5 is 5/6 of its volume at 0.2 GPa. At 10 GPa, $^{[4]}$T comprises only 10% of TO_n, with 50% of the units being TO_5 and about 35% of the T cations in octahedral coordination. The sum of the concentrations of $^{[4]}$T and $^{[5]}$T equals the abundance of $^{[6]}$T and the abundance of $^{[7]}$T equals the abundance of $^{[4]}$T (about 8%) at a pressure of 18 GPa. By 30 GPa, $^{[6]}$T at 47% surpasses the concentration of $^{[5]}$T (35%) and $^{[7]}$T (10%). The maximum concentration of octahedral T occurs at a compression ratio of 1.6, which corresponds to a pressure of 40 GPa where the molar volume is 5/8 of its low-pressure value. Clearly, there are profound changes in the short-range (smallest unit) structure characterized by variations in the abundance of TO_n as pressure increases. At the highest pressure, the concentrations of TO_7 and TO_8 are 30 and 10%, respectively. Although we know of no crystalline silicates with $^{[7]}$T or $^{[8]}$T, it is possible that such short range units do exist in molten anorthite. At the same time, we cannot rule out that their appearance is an artifact of the simple potential used in the simulations. It would be interesting to look for these

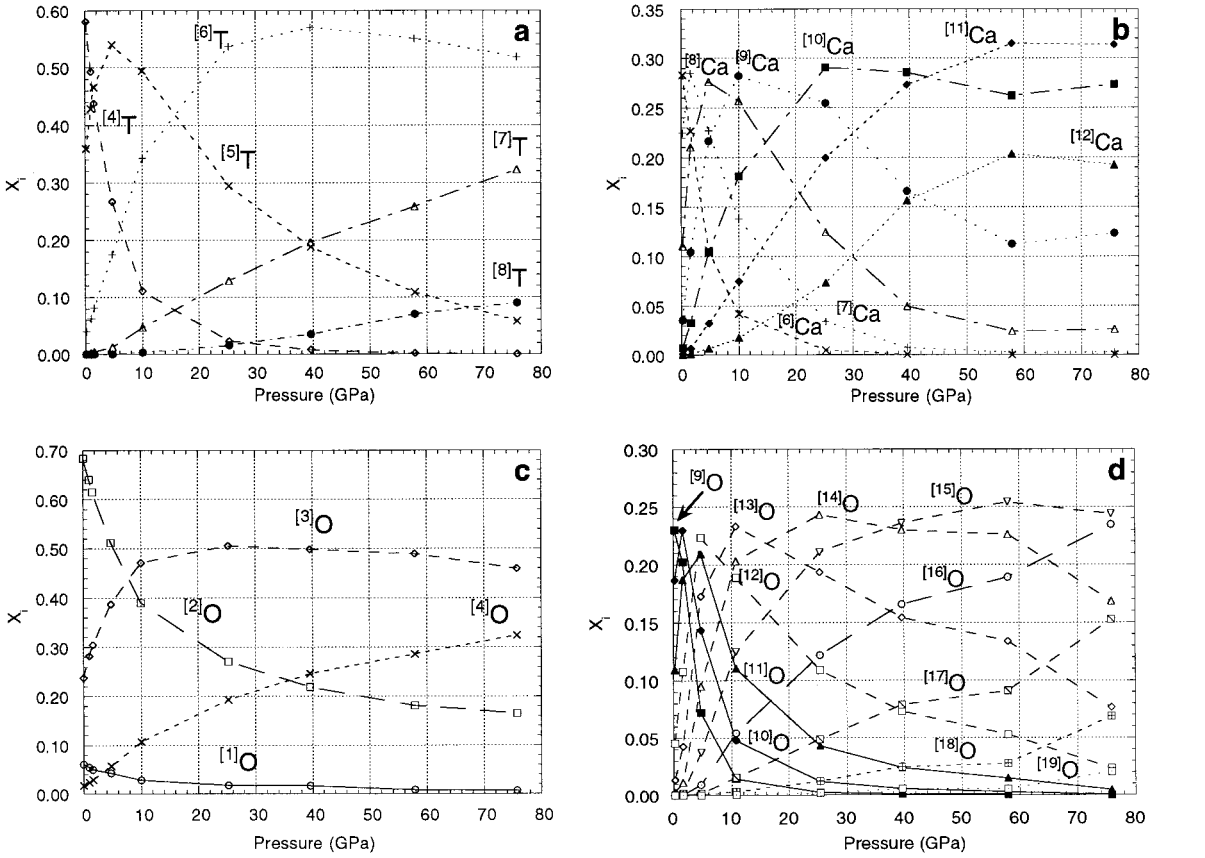

FIGURE 1. Concentration of short-range subunit species at 4000 K in MD simulations of molten $CaAl_2Si_2O_8$ vs. pressure. (**a**) Abundance expressed in terms of the number fraction of $AlO_4 + SiO_4 = {}^{[4]}T$, $AlO_5 + SiO_5 = {}^{[5]}T$, $AlO_6 + SiO_6 = {}^{[6]}T$, $AlO_7 + SiO_7 = {}^{[7]}T$ and $AlO_8 + SiO_8 = {}^{[8]}T$. Note the monotonic drop in ${}^{[4]}T$, the maximum in ${}^{[5]}T$ at 5 GPa and the monotonic growth of ${}^{[6]}T$, ${}^{[7]}T$, and ${}^{[8]}T$ as pressure increases. (**b**) CN of O about Ca. The average CN of O about Ca changes by a factor of two as pressure increases from 0.2 GPa to 76 GPa. (**c**) Number fraction of oxygen having one, two, three, or four nearest T neighbors. ${}^{[1]}O$ is equivalent to NBO, ${}^{[2]}O$ is the usual CN of T's about oxygen in network silicates at low pressure, ${}^{[3]}O$ represents an O atom shared by three subunits (not necessarily TO4s) and ${}^{[4]}O$ represents an O atom with four nearest T neighbors. (**d**) CN of O about O with ${}^{[n]}O$ ($5 \leq n \leq 8$) omitted for clarity.

subunits by in situ spectroscopic methods to sidestep the issue of TO_7 and TO_8 quenchability.

Analysis of O-T-O angles within TO_5 and TO_6 coordination polyhedra shows that average O-T-O angles vary only a few degrees with pressure. In contrast, ${}^{[4]}T$ average intra-tetrahedral O-T-O angles decrease from 109° at low pressure to 88° at 25 GPa where there are few (<5%) TO_4 present. The point is that TO_5 and TO_6 polyhedra evidently resist compression compared to TO_4. A steep decrease in the MD-computed isothermal compressibility of molten anorthite in the 0.2 to 10 GPa pressure interval correlates with the drop in abundance of the TO_4 unit from >60% to <10%; this leads to a collapse in the tetrahedral ring structure defined by TO_4 corner sharing polymerization (see below). The Brillouin scattering experiments of Askarpour et al. (1993) show that the configurational contribution to the compressibility of molten $CaAl_2Si_2O_8$ far exceeds the thermal (vibrational) component. This is clearly consistent with the dramatic changes in short and intermediate range structures determined by the MD simulations.

The coordination number of O about Ca systematically increases (Fig. 1b). In crystalline anorthite at low pressure, Ca is in irregular six- to sevenfold coordination with oxygen. At 0.2 GPa, the average coordination number is about 6.5 (15% ${}^{[5]}Ca$, 26% ${}^{[6]}Ca$, 32% ${}^{[7]}Ca$, and 19% ${}^{[8]}Ca$); this value steadily increases so that at 75 GPa the average coordination number is close to 11 (Fig. 1b). The low-pressure MD results are consistent with the arguments of Taylor and Brown (1979) who assert that Ca occupies a sevenfold-coordination site in glassy $CaAl_2Si_2O_8$ at 1 bar.

The coordination of oxygen around other O atoms is shown in Figure 1d. As pressure rises, the average CN of O increases rapidly from about 9 at 0.2 GPa, through 13 at 11 GPa, and then slowly climbs toward a maximum of about 15 at 76 GPa. The pressure interval of most rapid increase in the oxygen by oxygen CN is approxi-

mately the same as where the abundance of TO_5 and oxygen self-diffusivity attains a maximum. At the highest pressure of our simulations, oxygen approaches face-centered cubic closest packing.

Four principal environments occur for oxygen relative to the T cations: $^{[1]}$O, $^{[2]}$O, $^{[3]}$O, and $^{[4]}$O (Fig. 1c). At low pressure, most of the oxygen has two nearest T neighbors although 25% of the oxygen is in threefold coordination associated with TO_5 and about 6% of the oxygen is $^{[1]}$O or NBO. The appearance of NBOs in anorthite glass was observed by Stebbins and Xu (1997) who detected 4 to 5% NBOs by NMR spectroscopy on glassy anorthite. The predominance of mixed $^{[2]}$O and $^{[3]}$O is not unlike the situation in the aluminosilicate polymorphs sillimanite and andalusite. In the latter, AlO_4 chains are cross linked by Al in pairs of triangular O dipyramids (trigonal bipyramids) and by tetrahedral Si to form an Al-Al-Si oxygen tricluster consistent with $^{[3]}$O (see Fig. 12.11 in Jaffe 1996). This linkage is described by $^{[5]}$Al$^{-[3]}$O-$^{[4]}$Si and explains the steeper slope of $^{[3]}$O compared to $^{[6]}$T with increasing pressure noted by comparing Figures 1a and 1c. The maximum in $^{[3]}$O occurs at a compression ratio V_0/V equal to about 1.6 at 40 GPa at essentially the same pressure where $^{[6]}$T attains a maximum concentration. The concentration of $^{[4]}$O monotonically increases with pressure and reaches 30% (by number) at 76 GPa where the compression is close to 1.8 and the computed liquid molar volume of $CaAl_2Si_2O_8$ is 5/9 of its low pressure value. The increase in $^{[4]}$O at high pressure is indicative of oxygen in cubic close packing not unlike that in kyanite (Al_2SiO_5) in which 20% of the O atoms are $^{[4]}$O, the remaining being $^{[3]}$O.

The computed MD short-range structures noted above are consistent with the IR absorption study of Williams and Jeanloz (1988) and Williams (1998) on glassy anorthite at 300 K and pressures up to 37.6 GPa. They noted a gradual increase in the average CN from $^{[4]}$T to $^{[6]}$T in the range 10 to 20 GPa. The lack of discrete IR absorption peaks above 650 cm^{-1} in high-pressure anorthite glass suggested the virtual absence of $^{[4]}$T at pressures above 20 GPa and 300 K. As noted above, we find $<5\%$ $^{[4]}$T at pressures >20 GPa and 4000 K. Recognizing that kinetic hindrances are significantly reduced in melts compared to the glasses, Williams and Jeanloz (1988) hypothesized that coordination changes for melts would occur at lower pressures compared to the glass. This prediction is borne out by the MD simulations that show significant changes in short-range order at pressures approximately 2 to 5 GPa at 4000 K. Finally, we note that Williams and Jeanloz (1988) inferred the presence of $^{[5]}$Al from absorption bands between 600 to 900 cm^{-1} although they could not uniquely separate the contribution of $^{[5]}$Al from $^{[6]}$Si. The MD simulations predict that $^{[6]}$T becomes more abundant than $^{[5]}$T at pressures >15 GPa.

Intermediate range structures

To assess intermediate range order as a function of pressure, the statistics of the T-O-T distribution as well as the style of TO_n polyhedra linkage has been studied. For reference, a decrease in the most probable Si-O-Si angle with increasing pressure in glassy silica densified at 5 GPa and 873 K has been ascribed to a decrease in the O-second-nearest neighbor O separation from 3.12 to 2.95 Å by Devine et al (1987). These authors argue that the drop in the second nearest-neighbor distance modifies the distribution of possible network ring structures and permits the existence of low member rings generally associated with a smaller T-O-T angles (see also Galeener 1982a, 1982b). The effect recorded by Devine et al. (1987) on the most probable T-O-T angle is small; the modal T-O-T angle decreases from 143° to 138°. The main point is the obvious one: The T-O-T angle distribution is a reflection of the way polyhedra subunits are linked. The method of linkage essentially defines intermediate range order at scales from roughly 4 to 10 Å in network silicates. This differs from non-network silicates where topological changes can preserve the basic tetrahedral coordination and linkage (Kubicki et al. 1992).

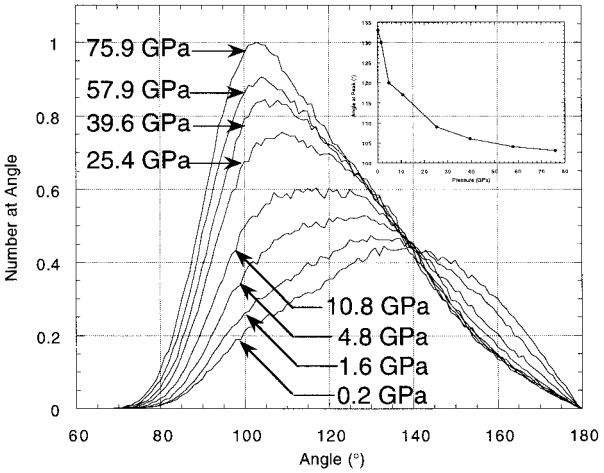

FIGURE 2. T-O-T angle distribution at 4000 K as a function of pressure from MD simulations on molten $CaAl_2Si_2O_8$. The T-O-T angle provides information on how TO_n subunits are linked. X-ray studies on glassy anorthite at 1 bar and 300 K give a T-O-T angle of 143° (Taylor et al. 1979), which can be compared with the MD-generated value of 135° at 0.2 GPa and 4000 K (see inset). The decrease in both the average T-O-T angle and the variance of the T-O-T angle distribution with increasing pressure reflects the destruction of the four- to eight-membered TO_4-based ring structure and the increasing proportion of edge-sharing TO_6 octahedra at high pressure. The range of ring sizes makes for the wider variance of the T-O-T angle distribution at low pressure. In contrast, edge-sharing TO_6 octahedra restrict the possible range of T-O-T angles due to the geometric constraints imposed by octahedral edge sharing.

The normalized T-O-T angle histogram (Fig. 2) shows a remarkable and large variation in the most probable T-O-T angle, as well as the higher moments of the T-O-T distribution as pressure increases. At 0.2 GPa, the distribution forms a broad maximum around 138° with a full width at half peak of 67°. X-ray experiments by Taylor

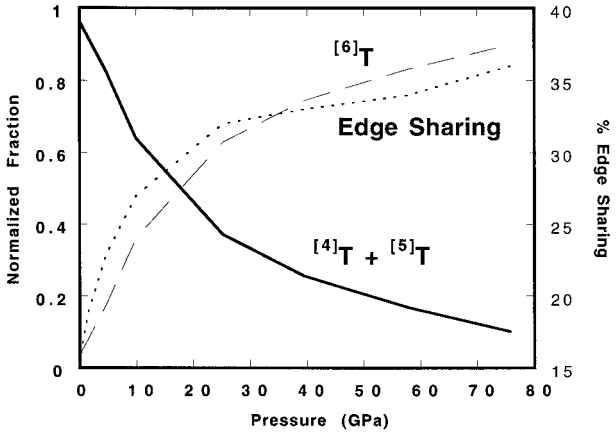

FIGURE 3. The calculated number fraction abundance of $^{[6]}T$ (dashed curve) and $^{[4]}T + {}^{[5]}T$ (solid curve) normalized to unity and plotted against pressure at 4000 K for $CaAl_2Si_2O_8$. Dotted curve, the number fraction of edge-sharing TO_n polyhedra. The correlation of the fraction of polyhedra that take part in edge sharing with abundance of $^{[6]}T$ is consistent with the distribution of T-O-T angles in Figure 2.

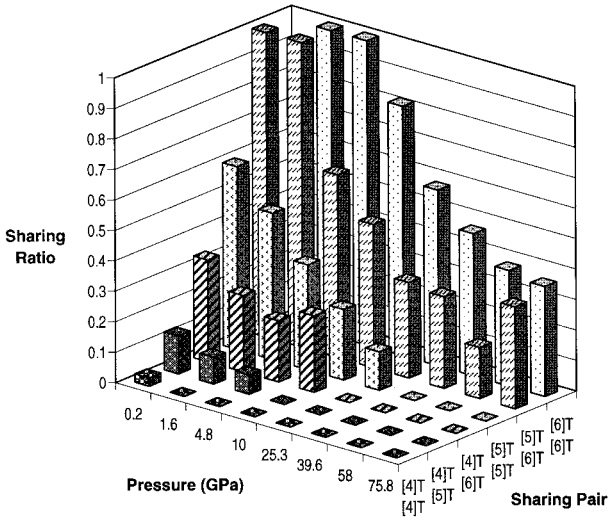

FIGURE 4. Calculated sharing ratios for selected TO_n polyhedra as a function of pressure. The sharing ratio for a given polyhedra pair (e.g., $^{[6]}T$-$^{[6]}T$) is defined as the ratio of the number of TO_6-TO_6 pairs that corner share to the number of TO_6-TO_6 pairs that edge share. The propensity of edge sharing in any polyhedra pair involving at least one TO_6 subunit is clearly seen as is the ability of TO_5 polyhedra to actively take part in corner sharing preferentially with TO_4 and edge-sharing with TO_6.

and Brown (1979) give a T-O-T angle of 143° for glassy anorthite at room temperature and 1 bar pressure. The most probable T-O-T angle rapidly drops from 140° at 0.2 GPa to about 120° around 5 GPa and then continues to decrease but at a decreasing rate to 117° at 10 GPa, 108° at 20 GPa, and asymptotically approaches about 105° for the highest pressure simulation at 76 GPa. The decrease of the T-O-T angle with pressure follows the form of the variation of $^{[2]}O$ (Fig. 1c); a rapid initial decrease followed by continued decrease but at a smaller rate.

A simple explanation of the behavior of the T-O-T angle distribution with increasing pressure is derived from the O sharing-statistics between discrete TO_n subunits ($4 \leq n \leq 8$) and considering the ways they may be linked. A given subunit is linked to another subunit, which may or may not be of the same type, either by sharing a corner O, sharing an edge (two Os shared per pair of subunits) or, very rarely, sharing of a polyhedra face. Face sharing of TO_n polyhedra is very rare even at 76 GPa and not considered further. Figure 3 shows a plot of the fraction of TO_n polyhedra that take part in edge sharing (regardless of speciation) vs. pressure. For low pressure, about 0.2 GPa, >85% of the subunits share corners with each other. As pressure increases there is a rapid rise in edge sharing that correlates with the increase of $^{[6]}T$. At the highest pressures, about 76 GPa, $^{[6]}T$ no longer increases in absolute terms (see Fig. 1a) but edge sharing still increases though at a much slower rate.

The amphoteric nature of $^{[5]}T$ as well as the proclivity of TO_6 to edge share is noted by examining the style of sharing (corner or edge) between TO_4, TO_5, and TO_6 polyhedra. This is done by studying the statistics of polyhedra linkage by calculation of the edge-sharing ratio defined to be the ratio of the number fraction of edge-sharing polyhedra divided by the fraction of corner-sharing polyhedra at the same pressure. This ratio indicates the tendency polyhedra have toward edge sharing. For example, Figure 4 shows that at 1.6 GPa the sharing ratio of the pair $^{[5]}T$-$^{[6]}T$ is 1.0, that is just as many $^{[5]}T$ share edges with $^{[6]}T$ as there are $^{[5]}T$ share corners with $^{[6]}T$. Examination of the sharing ratio for the pairs $^{[4]}T$-$^{[4]}T$, $^{[4]}T$-$^{[5]}T$, and $^{[4]}T$-$^{[6]}T$ reveals that for $^{[4]}T$-$^{[4]}T$ the sharing ratio is very low. The pairs $^{[4]}T$-$^{[5]}T$ and $^{[4]}T$-$^{[6]}T$ show a somewhat greater tendency for edge sharing than corner sharing.

In contrast, the sharing ratio for sharing pairs involving $^{[6]}T$ are much larger than most other combinations. In fact, the sharing pair $^{[6]}T$-$^{[6]}T$ has the greatest proclivity toward edge sharing relative to any other sharing pair. Edge-sharing polyhedra pairs interfere with the ring structure of the melt; this results in ring destruction as $^{[6]}T$ becomes quantitatively dominant. Sharing pair combinations involving $^{[5]}T$ are intermediate between $^{[4]}T$ and $^{[6]}T$. The sharing pair $^{[4]}T$-$^{[5]}T$ has a much lower sharing ratio than the sharing pair $^{[5]}T$-$^{[6]}T$. This means that $^{[5]}T$ prefers to share edges when it is combined with a $^{[6]}T$ but when combined with a $^{[4]}T$, $^{[5]}T$ prefers to share corners. The amphoteric nature of $^{[5]}T$ supports the idea that the $^{[5]}T$ acts like a $^{[4]}T$ when combined with $^{[4]}T$ and helps preserve the ring structure of molten anorthite. The amphoteric quality of the TO_5 subunit can also be appreciated by noting that at low pressure the fraction of edge-sharing polyhedra exceeds the concentration of $^{[6]}T$ whereas the opposite is true at pressure above 35 GPa as depicted in Figure 3.

Simple trigonometric calculations based on tetrahedral,

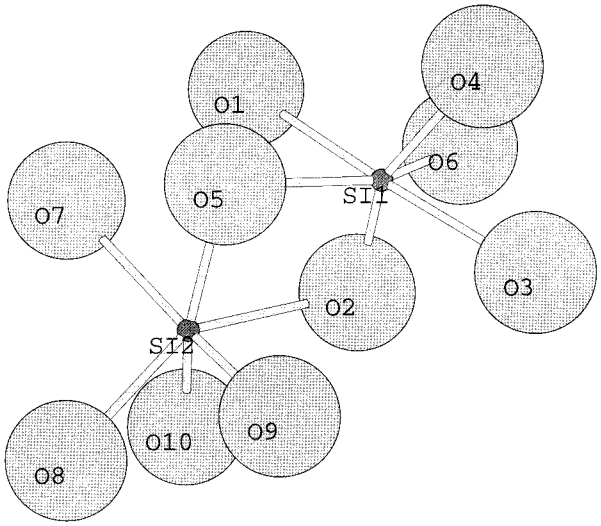

FIGURE 5. Oblique view of a pair of edge-sharing [6]T from an MD simulation at 25.3 GPa and 4000 K. The O-T-O angle O_5-Si_1-O_2 is 89.4° and the O-T-O angle O_5-Si_2-O_2 is 73.7°. The Si-O-Si angle is either 101° (Si_1-O_5-Si_2) or 92.2° (Si_1-O_2-Si_2). The ions O2, O4, O5, O6, O8, and O10 are approximately coplanar.

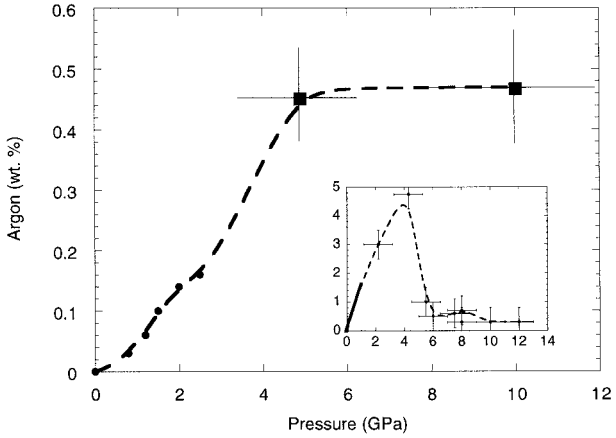

FIGURE 6. Solubility of Ar in molten anorthite from White et al (1989), shown by the solid circles, and Chamorro-Perez et al (1996), shown by the solid squares, at approximately 2000 K as a function of pressure. The pressure dependence of the solubility approaches zero in the same pressure interval that the TO_4-based ring structure is destroyed as edge-sharing TO_5 and TO_6 polyhedra dominate the system. Inset shows solubility relations in molten silica from Carroll and Stolper (1991) for comparison. This figure is modified from Figures 4 and 7 in Chamorro-Perez et al (1996).

trigonal bipyramidal, and octahedral subunits with T-T, T-O, and O-O bond distances determined from MD-generated pair correlation data suggests that rings made up of TO_4 and TO_5 subunits are characterized by T-O-T angles in the range 136 to 158° [T-O-T angle equals $2\sin^{-1}(d_{T-1}/2d_{T-0})$]. The span is wide because of the different bond lengths of Si-O and Al-O. Using the planar ring analysis of Galeener (1982a), trigonal bipyramidal rings have a maximum T-O-T angle of 180° for six-member rings with angles decreasing toward 120° as rings become smaller or larger. As pressure increases and the fraction of TO_6 increases at the expense of TO_5 and especially TO_4 (see Fig. 1), the fraction of edge-sharing subunits increases markedly. At the highest pressure of this study (approximately 76 GPa), about 35% of all subunits link by edge sharing and over 90% of the subunits are either TO_6 (52%), TO_7 (32%), or TO_8 (9%); the small coordination polyhedra TO_4 and TO_5 make up <6% of the total. Because TO_6 subunits are abundant at pressures >20 GPa, the second O-O nearest neighbor separation is expected to be $d_{O-O2} = \sqrt{2}d_{O-O1}$. This is verified by examination of the O-O pair correlation function; at pressures of 0.2, 1.6, 4.8, and 10.8 GPa, the second O-O distance is 5.2 Å as expected for a ring network of corner linked TO_4 and TO_5 units. At pressures of 25.4, 39.6, 57.9, and 75.9 GPa, however, the second O separation distance is 3.5 Å, which is close to $\sqrt{2}d_{O-O1}$ (3.53 Å) as expected for edge-sharing octahedra. A further consequence of the abundance of edge-sharing TO_6 octahedra is that the most probable T-O-T angle will decrease. A simple trigonometric construction shows that for regular octahedra the T-O-T angle $2\sin^{-1}(d_{T-T1}/2d_{T-O})$, is 129° for SiO_6 edge-sharing octahedra and 108° for AlO_6 edge-sharing octahedra based on bond distances recorded from pair correlations at high pressure. Figure 5 shows a pair of edge-sharing [6]Si taken from an MD experiment. The somewhat lower Si-O-Si angles are due to distortion of the edge-sharing octahedra.

Argon solubility

The idea that noble gases in network silicate melts reside in voids defined by the tetrahedral ring structure has been studied using modeling (e.g., Frenkel 1946; Shackelford et al. 1972; Shackelford and Masaryk 1978; Mitra 1982) and experiment (e.g., Barrer and Vaughan 1967; Studt et al. 1970; Shelby 1976; Carroll and Stolper 1991; Roselieb et al. 1995). MD simulations by Mitra (1982) showed that holes or noble gas sites defined by rings in computer SiO_2 melt at 3000 K were of sufficient size and abundance to effectively model the noble gas solubility characteristics of molten and glassy silica. More recent MD simulations on molten silica using both two and three body potentials (Feuston and Garofalini 1988; Kubicki and Lasaga 1988; Della Valle and Andersen 1992) indicate that the average ring size in high-temperature molten silica is six (about 30%) with the majority of other rings being five, seven, or eight membered. By definition, an *N*-membered ring contains *N* silicon atoms (or *N* tetrahedra) where silicon neighbors in the ring are connected through bridging oxygen.

If noble gases reside in ring-defined sites (holes), then the variation of solubility with pressure ought to be a sensitive indicator of melt structure. In Figure 6, Ar solubility data for molten SiO_2 (inset) and $CaAl_2Si_2O_8$ as a function of pressure determined by Carrol and Stolper (1991), White et al. (1989), and Chamorro-Perez et al.

(1996) are presented. For silica, Ar solubility goes through a maximum at about 4 GPa, consistent with MD simulations (Rustad et al. 1990; Rustad et al. 1991a, 1991b, 1991c; Rustad et al. 1992). These simulations showed that [5]Si and [6]Si become increasingly abundant at the expense of [4]Si as pressure increases. As noted above, [6]Si and to a lesser extent [5]Si are not good ring formers (i.e., they show preference for edge sharing opposed to corner sharing). MD simulations predict that as pressure increases the number of noble gas sites and hence gas solubility will decrease. Although solubility data for molten $CaAl_2Si_2O_8$ is sparser than for silica, it appears that the Ar solubility flattens in the 5 to 10 GPa pressure interval. This correlates very well with the previously presented MD-generated structure at both short and intermediate range. At low pressure, molten anorthite is dominated by [4]T arranged primarily into four- to six-member rings (Taylor and Brown 1979). As pressure increases, the [4]T first deform and then transform, after sufficient deformation, into [5]T. Chamorro-Perez et al. (1996) and White et al. (1989) observe the solubility of Ar to increase in the interval 0 to 4 GPa. On the basis of the MD simulations, we suggest that [5]T produced by the conversion of [4]T still exhibits some of the ring-former behavior of the [4]T. This enables the ring structure to survive the pressure increase and allow Ar to exhibit Henry's Law behavior of increasing solubility with increasing pressure. The solubility increases until around 5 GPa, the same pressure at which the concentration of [5]T maximizes. Above 5 GPa, the concentration of [6]T rapidly increases compared to [4]T and [5]T. The [6]T subunit acts like a ring defect and eventually the ring structure collapses and the Ar solubility departs radically from Henrian behavior. We predict that at pressures >5 GPa Ar solubility will monotonically decrease with increasing pressure.

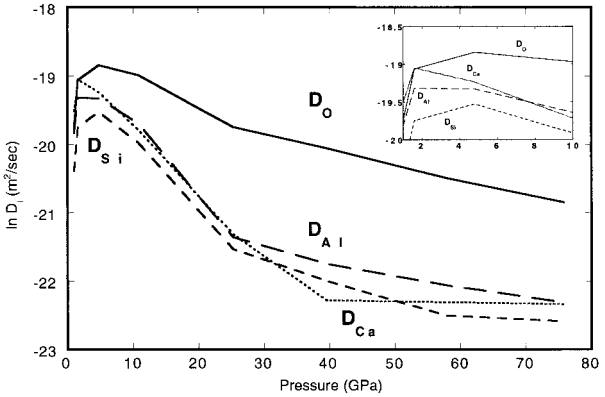

FIGURE 7. Tracer diffusivities for O, Al, Si, and Ca computed at 4000 K vs. pressure. Up to a few gigapascals, the activation volume for all ions is large and negative and varies from −15 to −38 cm³/mol. The diffusivity of O reaches a maximum at 5 GPa identical to the pressure at which [5]T is a maximum. The similarity in D values for Si, Al, and Ca is suggestive of cooperative diffusion. O remains the most mobile ion at all pressures. At high pressure, the diffusion of all ions is non-anomalous and the activation energy is quite small, around 1 to 3 cm³/mol.

Diffusion

The self-diffusion coefficient or tracer diffusivity D_i, for each species (Si, Al, O, Ca) can be computed from MD data using the Einstein relation:

$$D_i = \lim_{t\to\infty} \frac{\langle r_i(t) - r_i(0)\rangle^2}{6t} \quad (2)$$

This expression finds the slope in the limit as time t goes to infinity of the mean square displacement (MSD) for a given species; r is the position of the i^{th} atom and the bracket denotes that an ensemble average over many origin times has been taken (about 100 origin times within the 30 ps interval). In practice, MSD data are linearly regressed against time and the slope and its uncertainty are used to estimate D_i and its uncertainty.

Calculated tracer diffusivities for all species at 4000 K initially increase with pressure (see inset to Fig. 7). Using the simple Arrhenian formalism, the relation between diffusivity and pressure at fixed temperature is given by $D = D_0 \exp(-V_aP/RT)$ where D_0 is a constant at fixed temperature, V_a is the activation volume, R is the gas constant (8.3144 J/(mol·K) and T is the temperature. The positive slope found for each species implies so-called anomalous diffusion occurs in molten $CaAl_2Si_2O_8$ at low pressure; that is, diffusivity increases as pressure increases. Another way of expressing this is to note that all species at low pressure have a negative activation volume (V_a). Extrapolated to 1 bar pressure, V_a for Si, Ca, Al, and O are −15.2 cm³/mol, −25.4 cm³/mol, −28.3 cm³/mol, and −38.6 cm³/mol, respectively. We speculate that these relatively large absolute values for V_a are due to the open nature of the TO_4-dominated ring structure. MD computed values of the isothermal compressibility show a rapid decrease at low pressure and is correlated with the collapse of the open TO_4-based ring structure as TO_4 abundance drops and TO_5 and TO_6 abundances increase.

Examination of the inset to Figure 7 shows that the tracer diffusivity of Al and Ca each maximize at 2 GPa whereas the diffusivity of both Si and O maximize at 5 GPa. This suggests cooperative diffusive behavior. We speculate that in the case of Al and Ca, cooperativity originates in the tendency of Ca to associate with Al-bearing subunits (e.g., AlO_4, AlO_5, AlO_6) rather than analogous Si -bearing ones (e.g., SiO_4, SiO_5, SiO_6). In the case of O and Si at low pressure (greater than several Gigapascals), the mobility of O and Si perhaps are linked via the SiO_n subunit. The relatively large values for V_a of all species suggests that the activated volume involved in species diffusion is of the order of the volume of a TO_n subunit.

The pressure at which oxygen diffusion attains a maximum (5 GPa, Fig. 7) is identical, within error, to the pressure at which the concentration of [5]T maximizes (Fig. 1). This suggests that pentahedrally coordinated T acts as an ''activated complex'' for oxygen diffusion as hypothesized by several authors (e.g., see Brawer 1985;

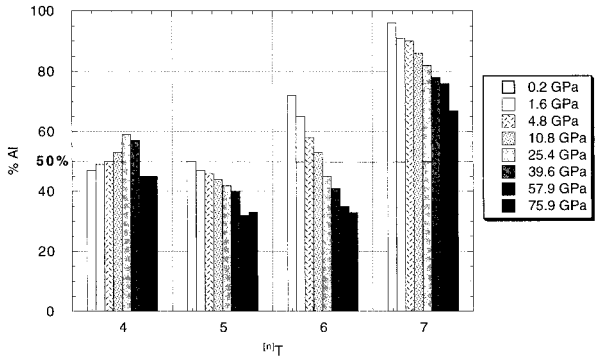

FIGURE 8. Aluminum fractionation of [4]T, [5]T, [6]T, and [7]T. Percentage of aluminum for a given [n]T is given as the percentage of all [n]T coordinated subunits that are aluminum for all time steps in a simulation experiment. For dominant [n]T, i.e., [4]T at low pressure and [6]T, [7]T at the higher pressures, the number of subunits found across the entire simulation is usually >15 000. For non-dominant [n]T, there is usually <3000 subunits for the entire simulation.

Kubicki and Lasaga 1988; Wolf et al. 1990; Xue et al. 1991; Poole et al. 1995; Poe et al. 1997). Poe et al. (1997) proposed that the maximum in the tracer diffusivity of oxygen observed experimentally in molten $NaAlSi_3O_8$ at 5 GPa is due to formation of a TO_5 by capture of an oxygen from an AlO_4, and that such preferential capture ultimately leads to exhaustion of AlO_4 and, hence, the turnover in the oxygen diffusivity. To examine this possibility, we gathered statistics on the fractionation of Al and Si as a function of pressure for the various TO_n polyhedra. In Figure 8, the fraction of TO_n polyhedra composed of Al are shown for various pressures. If the Poe et al. hypothesis is extended to $CaAl_2Si_2O_8$, then the fraction of AlO_4 near 4.8 GPa ought to be rapidly decreasing relative to SiO_4. This is not shown by the MD simulations. The plot shows that as pressure increases Si is preferentially accepted into TO_5 and TO_6 whereas Al prefers to enter the TO_7 polyhedra. Overall, fractionation effects are rather small in TO_4, TO_5, and TO_6 especially at pressures <20 GPa. The exception is for the TO_7 polyhedra that show, at all pressures, a strong tendency to fractionate Al from Si such that TO_7 is enriched in Al. Figure 1c shows that about equal amounts of [2]O and [3]O exist at 5 GPa.

As pressure is raised above 5 GPa, all tracer diffusivities decrease. Oxygen is the fastest species at all pressures studied. Al, Si, and Ca have equal mobilities about ten times slower than oxygen. For example, at 30 GPa, the diffusivity of Al, Ca, and Si is 4.6×10^{-10} m²/s whereas the oxygen tracer diffusivity is 2.5×10^{-9} m²/s. Activation volumes are positive at all pressures >5 GPa. At high pressure, the activation volume for tracer diffusion for all species is small (i.e., diffusion in nearly independent of pressure) and lies between +1 to +3 cm³/mol; anomalous diffusion disappears for Ca at 2 GPa and for the other species at 5 GPa.

The most abundant coordination polyhedra of oxygen about calcium increases rapidly from [6]Ca to [9]Ca in the pressure interval 0.2 to 10 GPa. The higher CN of Ca with oxygen is evidently not conducive to Ca mobility. Ca tracer diffusivity peaks near 2 GPa (Fig. 7) where the predominant coordination polyhedra are CaO_6, CaO_7, and CaO_8.

DISCUSSION

The simple pair-potential due to Scamehorn and Angell (1992) used in this study is reasonably successful in reproducing several characteristics of molten $CaAl_2Si_2O_8$. Recent NMR results by Stebbins and Xu (1997) suggest that, at low pressure, 4 to 5% of the oxygen is NBO (i.e., [1]O) in glassy anorthite. This compares with the MD prediction of about 5% (see Fig. 1c). Similarly, the predicted maximum in [5]T at 5 GPa is consistent with NMR results of Yarger et al. (1995) on a 50:50 $NaAlSi_3O_8$-$Na_2Si_4O_9$ melt at 2500 K, which exhibited a maximum of [5]Al at 8 GPa when allowance is made for the higher concentration of NBOs in the soda-rich composition compared to molten anorthite. The maximum observed in the solubility of argon with pressure can also be rationalized by the MD results. The observed maximum in the tracer diffusivity of oxygen at 5 GPa coincides with the maximum abundance (55%) of [5]T at this same pressure. This supports the idea that structural relaxation associated with diffusion of oxygen (and hence viscous flow) occurs through formation of a transient fivefold-coordinated T species.

There are several important geophysical implications of this work. Assuming they are not just an artifact of the simple potential, the identification of sevenfold- and eightfold-coordination states for Si and Al in melts, but not in corresponding crystalline compounds, may be relevant to the observation that at high pressure some melts become denser than their corresponding crystalline analogs. This may have significant implications for mantle differentiation especially during the early part of Earth history when a magma ocean may have been present and perhaps even today given recent identification of an ultralow velocity zone near the core-mantle boundary at 135 GPa (Williams and Garnero 1996). Similarly, the simulations predict that noble gasses such as argon may exhibit compatible geochemical behavior at high pressure due to profound changes in melt structure. This could effect models of noble gas exchange and terrestrial atmosphere evolution that seek to rationalize exchanges between various mantle reservoirs.

Future work on the problems discussed in this study should proceed along two fronts. In the temporal domain, it will be important to study the dynamical lifetimes of the various subunits. For example, we would like to know if the TO_5 species has a shorter lifetime than say a TO_4 or TO_6 species. The viscous relaxation time of the melt ought to correspond to the average lifetime of the average species the abundance of which, as shown here, depends on pressure. It also will be interesting to study changes in the structure and properties of $CaAl_2Si_2O_8$ as approach

is made to the glass transition along an isobar. A second future direction will be to study much larger (bigger N) systems. As we have shown, short-range order is faithfully captured by a simple effective pair potential. For the typical simulation of 1300 particles at 5 GPa, the size of the primary MD cell is about 26 Å. Because many 1 to 3 Å features fit inside a primary MD cell of this size, short range order can be successfully determined. However, intermediate-range structures, of length scale 3 to 10 Å, cannot be determined to the same extent as short-range order. The obvious direction then is to increase the size of the MD cell by increasing the number of particles to order $>10^5$. This practically requires the use of a force algorithm that scales as order N rather than order N^2.

ACKNOWLEDGMENTS

We are grateful to J. Bryce, J. Stebbins, D. Stein, A. Trial, and D. Yuen for many stimulating discussions. We would also like to express our appreciation to editor A. Hofmeister, associate editor L. Stixrude and two anonymous reviewers who markedly improved this paper with their suggestions. This research was partially funded by D.O.E. grant DE-FG03-91ER14211, N.S.F. grant EAR-9627800, and is Institute for Crustal Studies contribution number 0296-46CM. F.J.S. dedicates this paper to the memory of his father.

REFRENCES CITED

Allen, M.P. and Tildesley, D.J. (1987) Computer simulation of liquids. Oxford University Press Inc., New York.

Askarpour, V., Manghnani, M., and Richet, P. (1993) Elastic properties of diopside, anorthite, and grossular glasses and liquids: a Brillouin scattering study up to 1400 K. Journal of Geophysical Research, 98, 17683–17689.

Bansal, N. and Doremus, R (1986) Handbook of glass properties, 680 p. Academic Press, New York.

Barrer, R.M. and Vaughan, D.E.W. (1967) Solution and diffusion of helium and neon in tridymite and cristobalite. Transactions of the Faraday Society, 63, 2275–2290.

Brawer, S.A. (1985) A theory of dense liquids based on Monte Carlo simulations of very small clusters. Journal of Chemical Physics, 82, 2092–2105.

Bryce, J., Spera, F.J., and Stein, D.J. (1997) Dependence of self-diffusivity on P and T in molten NaAlSiO: Comparison of laboratory and molecular dynamics experiments. Geophysical Research Letters, 24, 711–714.

Carroll, M.R. and Stolper, E.M. (1991) Argon solubility and diffusion in silica glass; implications for the solution behavior of molecular gases. Geochimica et Cosmochimica Acta, 55, 211–225.

Chamorro-Perez, E., Gillet, P., and Jambon, A. (1996) Argon solubility in silicate melts at very high pressures. Experimental set-up and preliminary results for silica and anorthite melts. Earth and Planetary Science Letters, 145, 97–107.

Della Valle, R. and Andersen, H.C. (1992) Molecular dynamics simulation of silica liquid and glass. Journal of Chemical Physics, 97, 2682–2689.

Devine, R.A.B. and Arndt, J. (1987) Si-O bond-length modification in pressure-densified amorphous SiO, Physical Review B (Condensed Matter), 35(17) 9376–9379.

Dowty, E. (1995) ATOMS, Version 3.1.1, Shape Software.

Feuston, B.P. and Garofalini, S.H. (1988) Empirical three-body potential for vitreous silica. Journal of Chemical Physics, 89, 5818–5824.

Frenkel, J. (1946) Kinetic theory of liquids, Dover, N.Y.

Galeener, F.L. (1982a) Planar rings in glasses, Solid State Communications, 44,(7) 1037–1040.

———(1982b) Planar rings in vitreous silica, Journal of Non-Crystalline Solids, 49, 53–62.

Gautron, L., Kesson, S.E., and Hibberson, W.O. (1996) Phase relations for $CaAl_2Si_2O_8$ (anorthite composition) in the system CaO-Al_2O_3-SiO_2 at 14 GPa. Physics of the Earth and Planetary Interiors, 97, 71–81.

Jaffe, H. (1996) Crystal chemistry and refractivity, Dover Publications, Mineola, New York

Kawamura, K. (1991) A Molecular Dynamics Simulation of $Na_2O{\cdot}2SiO_2$-$K_2O{\cdot}2SiO_2$ Melts-Effect of Basic Cell Size. Molecular Simulation, 6, 245–255.

Kubicki, J.D. and Lasaga, A.C. (1988) Molecular dynamics simulations of SiO_2 melt and glass, ionic and covalent models. American Mineralogist, 73, 941–955.

———(1993) Molecular dynamics simulations of interdiffusion in $MgSiO_3$-Mg_2SiO_4 melts. Physics and Chemistry of Minerals, 20, 255–262.

Kubicki, J.D., Hemley, R.J., and Hofmeister, A.M. (1992) Raman and infrared study of pressure-induced structural changes in $MgSiO_3$, $CaMgSi_2O_6$, and $CaSiO_3$ glasses. American Mineralogist, 77, 258–269.

Matsui, M. and Kawamura, K. (1984) Computer simulation of structures of silicate melts and glasses. In I. Sunagawa, Ed., Materials Science of the Earth's Interior, p. 3–23. Reidel, Boston.

McMillan, P.F. and Wolf, G.H. (1995) Vibrational spectroscopy of silicate liquids. In Mineralogical Society of America Reviews in Mineralogy, 32, 247–315.

Mitra, S.K. (1982) Molecular dynamics simulation of silicon dioxide glass. Philosophical Magazine B, Physics of Condensed Matter, Electronic, Optical and Magnetic Properties, 45, 529–548.

Poe, B.T., McMillan, P.F., Rubie, D.C., Chakraborty, S., Yarger, J., and Diefenbacher, J. (1997) Silicon and oxygen self-diffusivities in silicate liquids measured to 15 gigapascals and 2800 Kelvin. Science, 276, 1245–1248.

Poole, P.H., McMillan, P.F., and Wolf, G.H. (1995) Computer simulations of silicate melts. In Mineralogical Society of America Reviews in Mineralogy, 32, 563–616.

Roselieb, K., Rammensee, W., Buettner, H., and Rosenhauer, M. (1995) Diffusion of noble gases in melts of the system SiO_2-$NaAlSi_2O_6$. Chemical Geology, 120, 1–14.

Rustad, J.R., Yuen, D.A., and Spera, F.J. (1990) Molecular dynamics of liquid SiO_2 under high pressure. Physical Review A, 42(4), 2081–2089.

———(1991a) The sensitivity of physical and spectral properties of silica glass to variations of interatomic potentials under high pressure. Physics of the Earth and Planetary Interiors, 65, 210–230.

———(1991b) The statistical geometry of pressure-induced coordination modifications in amorphous silica. Eos, 72, 146.

———(1991c) The statistical geometry of amorphous silica at lower mantle pressures; implications for melting slopes of silicates and anharmonicity. Journal of Geophysical Research, B, Solid Earth and Planets, 96, 19,665–19,673.

———(1992) Coordination variability and the structural components of silica glass under high pressures. Chemical Geology, 96, 421–437.

Scamehorn, C.A. and Angell, C.A. (1991) Viscosity-temperature relations and structure in fully polymerized aluminosilicate melts from ion dynamics simulations. Geochemica et Cosmochemica Acta, 55, 721–730.

Shackelford, J.F. and Masaryk, J.S. (1978) The interstitial structure of vitreous silica. Journal of Non-Crystalline Solids, 30, 127–134.

Shackelford, J.F., Studt, P.L., and Fulrath, R.M. (1972) Solubility of gases in glass. II. He, Ne, and H_2 in fused silica. Journal of Applied Physics, 43, 1619–1625.

Shelby, J.E. (1976) Pressure dependence of helium and neon solubility in vitreous silica. Journal of Applied Physics, 47, 135–139.

Stebbins, J.F. and McMillan, P.F. (1989) Five and six-coordinated Si in $K_2Si_4O_9$ glass quenched from 1.9 GPa and 1200 °C. American Mineralogist, 74, 965–968.

Stebbins, J.F. and Xu, Z. (1997) Non-bridging oxygens in a ''framework'' aluminosilicate glass: oxygen-17 NMR results. Eos, 78, Fall Meeting Supplement, V12E-9.

Stein, D.J. and Spera, F.J. (1995) Molecular dynamics simulations of liquids and glasses in the system $NaAlSiO_4$-SiO_2: I: Methodology and melt structures. American Mineralogist, 80, 417–431.

———(1996) Molecular dynamics simulations of liquids and glasses in the system $NaAlSiO_4$-SiO_2; Physical properties and transport mechanisms. American Mineralogist, 81, 284–302.

Studt, P.L., Shackelford, J.F., and Fulrath, R.M. (1970) Solubility of gases

in glass—a monatomic model. Journal of Applied Physics, 41, 2777–2780.

Taylor, M. and Brown, G.E. (1979) Structure of mineral glasses; I, The feldspar glasses $NaAlSi_3O_8$, $KAlSi_3O_8$, $CaAl_2Si_2O_8$, Geochimica Cosmochimica Acta, 43(1) 61–77.

Vollmayr, K., Kob, W., and Binder, K. (1996) Cooling-rate effects in amorphous silica: a computer-simulation study. Physical Review B (Condensed Matter), 54, 15808–15827.

White, B.S., Brearley, M., and Montana, A. (1989) Solubility of argon in silicate liquids at high pressures. American Mineralogist, 74, 513–529.

Wolf, G.H. and McMillan, P.F. (1995) Pressure effects on silicate melt structure and properties. In Mineralogical Society of America Reviews in Mineralogy, 32, 505–562.

Wolf, G.H., Durben, D.J., and McMillan, P.F. (1990) High-pressure Raman spectroscopic study of sodium tetrasilicate ($Na_2Si_4O_9$) glass. Journal of Chemical Physics, 93, 2280–2288.

Woodcock, L.V., Angell, C.A., and Cheeseman, P. (1976) Molecular dynamics studies of the vitreous state: simple ionic systems and silica. Journal of Chemical Physics, 65, 1565–1577.

Williams, Q. (1998) High-pressure infrared spectra of feldspars: constraints on compressional behavior, amorphization, and diaplectic glass formation. In H. Manghnani and T. Yagi, Eds., Properties of Earth and Planetary Materials at High Pressure and Temperature, p. M531–M543. Geophysical Monograph 101.

Williams, Q. and Jeanloz, R. (1988) Spectroscopic evidence for pressure-induced coordination changes in silicate glasses and melts. Science, 239, 902–905.

Williams, Q. and Garnero, E.J. (1996) Seismic evidence for partial melt at the base of Earth's mantle. Science, 273, 1528–1530.

Xue, X., Stebbins, J.F., Kanzaki, M., McMillan, P.F., and Poe, B. (1991) Pressure-induced silicon coordination and tetrahedral structural changes in alkali oxide-silica melts up to 12 GPa; NMR, Raman, and infrared spectroscopy. American Mineralogist, 76, 8–26.

Yarger, J.L., Smith, K.H., Nieman, R.A., Diefenbacher, J., Wolf, G.H., Poe, B.T., and McMillan, P.F. (1995) Al coordination changes in high-pressure aluminosilicate liquid. Science, 270, 1964–1967.

Manuscript received February 5, 1998
Manuscript accepted July 15, 1998
Paper handled by Lars Stixrude